Impact of the Non-Negativity Constraint in Model-Based Iterative Reconstruction from CT Data

Viktor Haase[1,2], Katharina Hahn[2], Harald Schöndube[2], Karl Stierstorfer[2], Frédéric Noo[3]

[1]Pattern Recognition Lab, Department of Computer Science, Friedrich-Alexander-Universität Erlangen-Nürnberg, Erlangen, Germany
[2]Siemens Healthcare GmbH, Forchheim, Germany
[3]Department of Radiology and Imaging Sciences, University of Utah, Salt Lake City, Utah, USA

Introduction

- Model-based iterative reconstruction (MBIR) is promising for reducing CT radiation dose while maintaining image quality
- Shows strong potential for clinical applications [1],[2]
- MBIR formulation typically includes non-negativity constraint motivated by physics of X-ray attenuation
- Our focus: Impact of the non-negativity constraint on image appearance and convergence speed under different scenarios based on real CT data

Material and Methods

- Objective function:
  - Penalized least squares
  - Data fidelity as squared residual without statistical weights
  - Potential function is either quadratic or edge-preserving and is applied to voxel differences in x,y,z-direction
  - Non-smooth indicator function enforces non-negative values
- Optimization algorithm: FISTA with constant step size [3]

Results: Image Quality

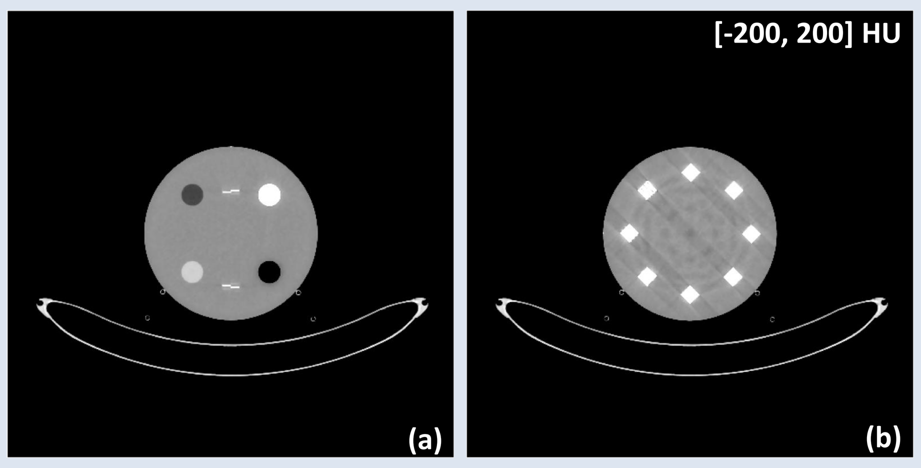

Figure 1: Ground truth of reconstruction with edge-preserving regularization and non-negativity constraint. Central z-slice of 3-D volume after 5000 iterations. (a) Module A of ACR phantom. (b) Module D of ACR phantom.

Full view sampling

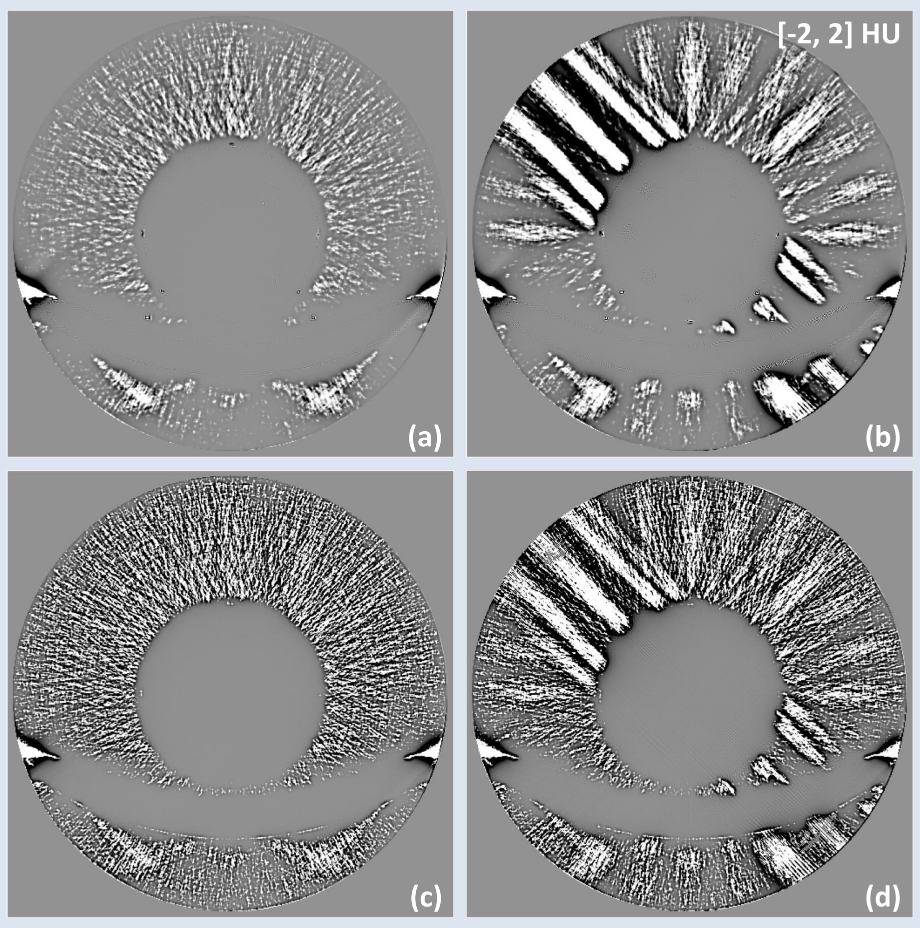

Table 1: Summary values of difference images. Measured inside the phantom, in HU.

Image	Min.	Max.	Mean	SD
(a)	-1.50	1.85	-0.02	0.03
(b)	-1.61	1.36	-0.09	0.09
(c)	-0.20	0.05	-0.05	0.03
(d)	-0.79	0.35	-0.12	0.10

Figure 2: Difference images for reconstruction with and without non-negativity constraint.
(a) Module A, edge-preserving reg.
(b) Module D, edge-preserving reg.
(c) Module A, quadratic reg.
(d) Module D, quadratic reg.

Sparse view sampling

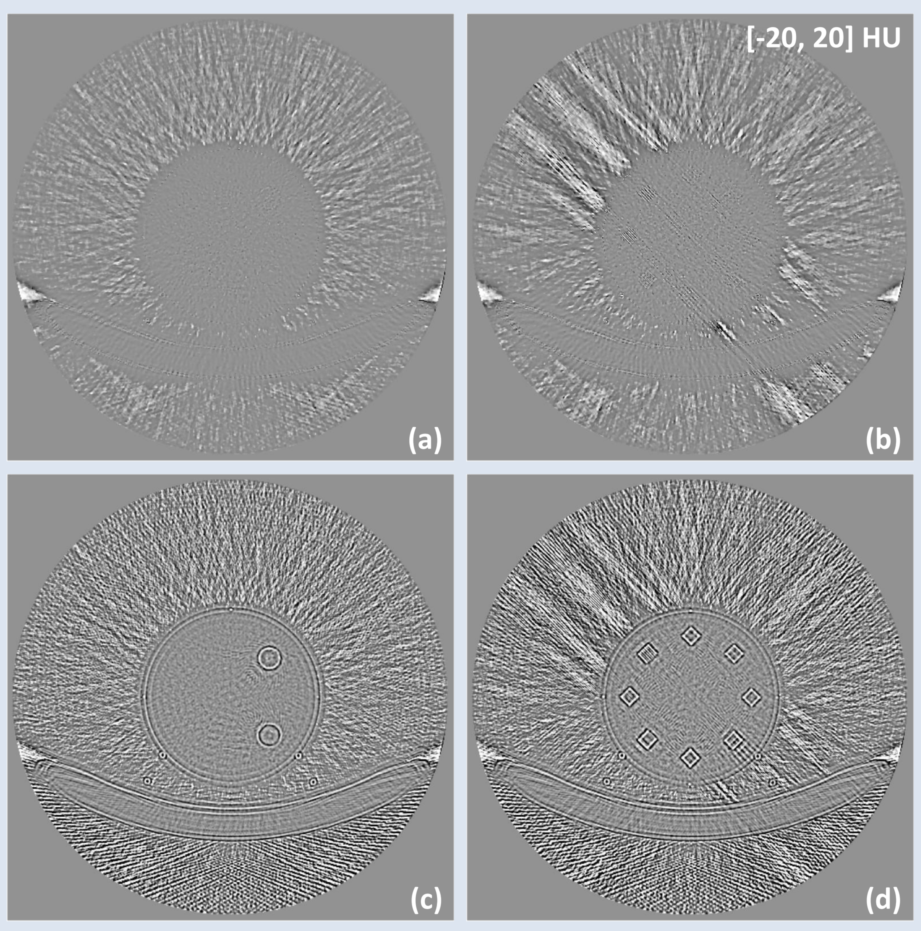

Table 2: Summary values, in HU.

Image	Min.	Max.	Mean	SD
(a)	-13.02	11.29	-0.08	1.09
(b)	-42.90	38.98	-0.16	3.56
(c)	-29.17	26.45	-0.14	3.77
(d)	-47.39	54.89	-0.26	7.01

Figure 3: Difference images, as above.

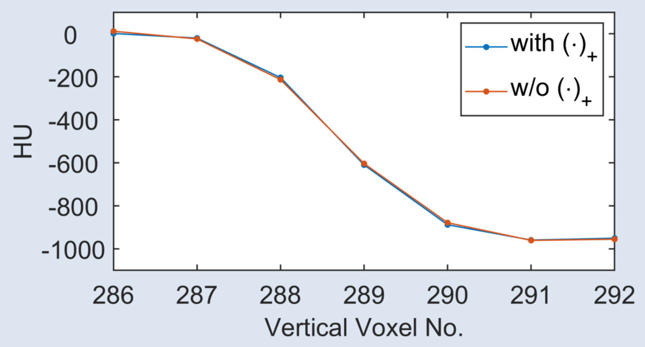

Figure 4: Profile plot for setting (c). Edge crossing from water to air, in HU.

Experimental Setup

- State-of-the-art clinical CT system using a 360° circular scan trajectory:

Source to detector distance	108.56 cm
Source trajectory radius	59.5 cm
Anode angle	7°
Number of detector channels	736
Angular detector width	0.067864°
Number of detector rows	8
Detector row height at isocenter	0.06 cm
Number of projections	2304 (full view sampling) 288 (sparse view sampling)
In-plane flying focal spot	on for full view sampling only
X-ray tube setting	80 kV at 500 mAs

- Reconstruction:

Number of iterations	5000
Volume size	512 x 512 x 16 voxels
Voxel size	0.1 x 0.1 x 0.06 cm
FOV radius	25.0 cm
FISTA step size	0.000065 (full view sampling) 0.00052 (sparse view sampling)
Hyperparameter β	0.1 (full view sampling) 0.0125 (sparse view sampling)
δ for quadratic reg.	0.005
δ for edge-preserving reg.	0.001

- Eight imaging scenarios:
  - Two test objects: ACR CT phantom module A for alignment and CT value accuracy, and module D for high contrast spatial resolution
  - Full view sampling or sparse view sampling of projection data
  - Edge-preserving or quadratic potential function for regularization

Results: Convergence Speed

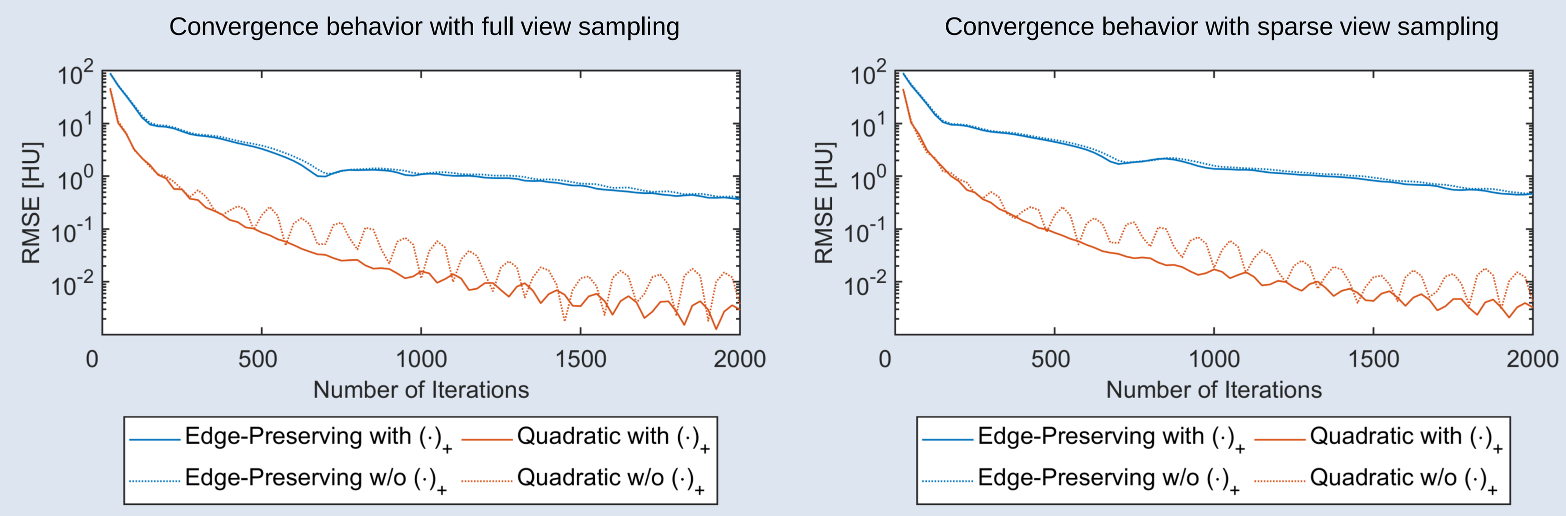

Figure 5: Convergence behavior for reconstruction of module A with *full view sampling* (left) and *sparse view sampling* (right). RMSE is calculated inside the phantom including its edges. Same curves are observed for module D.

Conclusions

- Non-negativity constraint might not offer any benefit for conventional diagnostic CT imaging
- Could help for reconstructions under challenging conditions like sparse view sampling
- Without non-negativity constraint simpler optimization algorithms are allowed which could result in less computational effort for the reconstruction
- Results have to be verified with a wider range of objective functions and optimization algorithms, and a more complex anthropomorphic object with several air cavities

Acknowledgement

This project was partly supported by Siemens Healthcare GmbH and partly by the National Cancer Institute of the National Institutes of Health under R21CA211035.

References

[1] Ichikawa, Y. et al., BMC medical imaging 13(1), 27 (2013).
[2] Desai, G. et al., European radiology 22(8), 1631–1640 (2012).
[3] Beck, A. et al., SIAM journal on imaging sciences 2(1), 183–202 (2009).

Contact

viktor.haase@fau.de
https://www5.cs.fau.de/~vhaase